

Universität des Saarlandes



Fachrichtung 6.1 – Mathematik

Preprint Nr. 228

**A Variational Multiscale Method for Turbulent Flow
Simulation with Adaptive Large Scale Space**

Volker John and Adela Kindl

Saarbrücken 2009

A Variational Multiscale Method for Turbulent Flow Simulation with Adaptive Large Scale Space

Volker John

Saarland University
Department of Mathematics
P.O. Box 15 11 50
66041 Saarbrücken
Germany
john@math.uni-sb.de

Adela Kindl

Saarland University
Department of Mathematics
P.O. Box 15 11 50
66041 Saarbrücken
Germany
adela@c-kindl.de

Edited by
FR 6.1 – Mathematik
Universität des Saarlandes
Postfach 15 11 50
66041 Saarbrücken
Germany

Fax: + 49 681 302 4443
e-Mail: preprint@math.uni-sb.de
WWW: <http://www.math.uni-sb.de/>

Abstract

In turbulent flows it is only feasible to simulate large flow structures. Variational multiscale (VMS) methods define these flow structures by projections into appropriate function spaces. This paper presents a finite element VMS method which defines the large scale projection space adaptively. The adaption controls the influence of an eddy viscosity model and it is based on the size of the so-called resolved small scales. The adaptive procedure is described in detail. Numerical studies at a turbulent channel flow and a turbulent flow around a cylinder are presented. It is shown that the method selects the large scale space in a correct way and that appropriately chosen parameters improve the results compared to the basic method, which uses the same local large scale space in the whole domain and for all times.

1 Introduction

Incompressible flows are governed by the incompressible Navier–Stokes equations which, in dimensionless form, read

$$\begin{aligned} \mathbf{u}_t - 2\nu\nabla \cdot \mathbb{D}(\mathbf{u}) + (\mathbf{u} \cdot \nabla)\mathbf{u} + \nabla p &= \mathbf{f} && \text{in } (0, T] \times \Omega, \\ \nabla \cdot \mathbf{u} &= 0 && \text{in } [0, T] \times \Omega, \\ \mathbf{u} &= \mathbf{0} && \text{in } [0, T] \times \partial\Omega, \\ \mathbf{u}(0, \mathbf{x}) &= \mathbf{u}_0 && \text{in } \Omega, \\ \int_{\Omega} p \, d\mathbf{x} &= 0, && \text{in } (0, T]. \end{aligned} \tag{1}$$

Here, $\Omega \subset \mathbb{R}^3$ is a bounded, connected domain with polygonal boundary $\partial\Omega$, $[0, T]$ is a finite time interval, \mathbf{u} is the fluid velocity, p is the pressure, \mathbf{f} is an external force, ν is the kinematic viscosity, \mathbf{u}_0 is the initial velocity field, and $\mathbb{D}(\mathbf{u}) = (\nabla\mathbf{u} + (\nabla\mathbf{u})^T)/2$ is the velocity deformation tensor (symmetric part of the gradient).

Turbulent flows are characterized by a multitude of different sizes for the flow scales, fact which makes the simulation of such flows by direct discretization generally infeasible with the currently available computer hardware. As the resolution of all flow scales is not possible, and the unresolved scales are important for the turbulent character of the flow, their influence onto the resolved scales needs to be taken into account via a turbulence model.

Popular methods for simulating turbulent flows include $k - \varepsilon$ models [27] and Large Eddy Simulation (LES) [30, 2]. In LES, the flow field is decomposed through spatial filtering and this method aims at an accurate simulation of only the so-called resolved scales. Widely used traditional LES models are Smagorinsky-type models [31, 6, 26].

As an alternative, Variational Multiscale (VMS) methods are a rather new approach for simulating turbulent flows. The basic idea of VMS methods, in contrast to traditional LES, is the use of variational projections instead of filtering for the scale decomposition, thus eliminating several difficulties of the traditional LES, e.g. commutation errors [5, 15,

3, 1]. VMS methods for turbulent flow simulations were derived from general principles for treating multiscale phenomena [11, 10]. For an introduction as well as a review to VMS methods and their relation and differences to traditional LES methods, we refer to [12, 13, 17]. There are meanwhile several realizations of VMS methods, see the reviews in [25, 21].

The present paper considers a three-scale VMS method, i.e. the flow is decomposed into three scales: large (resolved) scales, resolved small scales, and (small) unresolved scales. Assuming that the direct influence of the unresolved scales onto the large scales is negligible, and thus the direct influence of the unresolved scales is confined to the resolved small scales, the influence of the unresolved scales onto the resolved small scales is modeled with a turbulence model of eddy viscosity type. There is no direct turbulence modeling for the large scales, however the large scales are still influenced indirectly by the small unresolved scales due to the coupling of all three scales.

The considered VMS method uses finite elements as underlying spatial discretization, therefore it is called finite element VMS (FEVMS) method. The projection for the definition of the scales is contained explicitly in the set of equations. This projection-based FEVMS method was proposed in [18]. Its parameters are the finite element spaces used to define the scale decomposition and the turbulence model acting directly only on the resolved small scales. Regarding the turbulence model, the parameter in the additional viscous term added to the momentum equation is generally chosen to be an eddy viscosity model of Smagorinsky type [25, 20, 21]. Regarding the spaces, standard finite element spaces for the incompressible Navier–Stokes equations are used for all resolved scales and the separation of the large and the resolved small scales is achieved through an additional tensor-valued large scale space.

Available numerical studies [25, 20, 21] show that the choice of the additional large scale space has more influence on the results than changing the parameter in the eddy viscosity turbulence model. All these studies used globally uniform large scale spaces, i.e. the polynomial degree of the finite element tensors was the same for all mesh cells. This polynomial degree was chosen before starting the computations and it remained fixed during the simulations of the flows.

This paper will present an extension of the projection-based FEVMS method which computes the large scale space a posteriorily and adaptively. Firstly, it is no longer necessary to choose a large scale space for the whole simulation, the new method computes an appropriate large scale space during the simulation. Secondly, the large scale space may change during the simulation. This property is of importance if main features of the flow field change during the simulation. And thirdly, the large scale space is no longer uniform, different mesh cells may have finite element tensors with different polynomial degrees. This feature of the new method takes into account that in general the flow is not equally turbulent in the whole domain. There are subregions, e.g. at walls, with a strong turbulent character and in other subregions the flow behaves more or less laminar. With respect to the large scale space in the projection-based FEVMS method, the first situation corresponds to the necessity of using a locally small large scale space which allows a stronger influence of the eddy viscosity turbulence model. The second situation is vice versa.

The remainder of the paper is organized as follows: Section 2 introduces the considered projection-based FEVMS method. The adaptive algorithm for choosing the large scale space is described in detail in Section 3. A turbulent channel flow and a turbulent flow around a cylinder are studied in Section 4. Finally, Section 5 contains a summary of this paper.

2 Projection-Based Finite Element Variational Multiscale Methods

In the projection-based FEVMS method, all resolved scales belong to standard finite element spaces and an additional large scale space is needed for the scale separation. The resolved scales are decomposed into large and small ones with the help of a projection into the additional large scale space. The FEVMS method presented here contains this projection explicitly as an additional equation.

Let $V^h \times Q^h$ be a pair of inf-sup stable, conforming finite element spaces for the velocity and pressure. Consider an additional finite dimensional space of symmetric 3×3 tensor-valued functions $L^H \subset \{\mathbb{L} \in (L^2(\Omega))^{3 \times 3}, \mathbb{L}^T = \mathbb{L}\}$ representing a coarse or large scale space, and let ν_T be a non-negative function representing the turbulent viscosity. The semi-discrete (continuous in time) projection-based FEVMS method with parameters ν_T and L^H then seeks $\mathbf{u}^h : [0, T] \rightarrow V^h$, $p^h : (0, T] \rightarrow Q^h$, and $\mathbb{G}^H : [0, T] \rightarrow L^H$ such that

$$\begin{aligned} (\mathbf{u}_t^h, \mathbf{v}^h) + (2\nu\mathbb{D}(\mathbf{u}^h), \mathbb{D}(\mathbf{v}^h)) + ((\mathbf{u}^h \cdot \nabla)\mathbf{u}^h, \mathbf{v}^h) \\ - (p^h, \nabla \cdot \mathbf{v}^h) + (\nu_T(\mathbb{D}(\mathbf{u}^h) - \mathbb{G}^H), \mathbb{D}(\mathbf{v}^h)) &= (\mathbf{f}, \mathbf{v}^h), \quad \forall \mathbf{v}^h \in V^h, \\ (q^h, \nabla \cdot \mathbf{u}^h) &= 0, \quad \forall q^h \in Q^h, \\ (\mathbb{D}(\mathbf{u}^h) - \mathbb{G}^H, \mathbb{L}^H) &= 0, \quad \forall \mathbb{L}^H \in L^H. \end{aligned} \quad (2)$$

The tensor \mathbb{G}^H is the L^2 -projection of $\mathbb{D}(\mathbf{u}^h)$ into the large scale space L^H , representing the large scales of $\mathbb{D}(\mathbf{u}^h)$. Consequently, $\mathbb{D}(\mathbf{u}^h) - \mathbb{G}^H$ represents the resolved small scales. The additional viscous term $(\nu_T(\mathbb{D}(\mathbf{u}^h) - \mathbb{G}^H), \mathbb{D}(\mathbf{v}^h))$, introduced by the projection-based VMS methods in the momentum equation, acts directly only on the resolved small scales, and the main feature of a VMS method is hence recovered.

A crucial point for the results obtained with a projection-based FEVMS method of the form (2) is the choice of the large scale space $L^H \subseteq \{\mathbb{D}(\mathbf{v}^h) : \mathbf{v}^h \in V^h\}$. Since it has been distinguished between resolved small scales and large scales, with L^H representing the large scales, L^H must be in some sense a coarse finite element space. One way of achieving this is by choosing L^H to be a lower order finite element space than V^h , on the same grid, called one-level method. This requires that V^h is in some sense a higher order finite element space. An alternative consists in defining L^H on a coarser grid, see [19] for a discussion on one-level and two-level projection-based FEVMS methods. In the present paper, the one-level approach will be used.

The projection terms in (2) can be treated explicitly or implicitly in time, see [20]. We will restrict here to the implicit treatment, see [20] for comments on the explicit approach.

The fully implicit projection–based FEVMS method, discretized in time using a θ –scheme, reads: Find $(\mathbf{u}_K^h, p_k^h) \in V^h \times Q^h$ such that

$$\begin{aligned}
& (\mathbf{u}_k^h, \mathbf{v}^h) + \theta_1 \Delta t_k \left[((2\nu + \nu_{T,k}) \mathbb{D}(\mathbf{u}_k^h), \mathbb{D}(\mathbf{v}^h)) + ((\mathbf{u}_k^h \cdot \nabla) \mathbf{u}_k^h, \mathbf{v}^h) \right. \\
& \quad \left. - (\nu_{T,k} \mathbb{G}_k^H, \mathbb{D}(\mathbf{v}^h)) \right] - (p_k, \nabla \cdot \mathbf{v}^h) \\
& = (\mathbf{u}_{k-1}^h, \mathbf{v}^h) - \theta_2 \Delta t_k \left[((2\nu + \nu_{T,k-1}) \mathbb{D}(\mathbf{u}_{k-1}^h), \mathbb{D}(\mathbf{v}^h)) + ((\mathbf{u}_{k-1}^h \cdot \nabla) \mathbf{u}_{k-1}^h, \mathbf{v}^h) \right. \\
& \quad \left. - (\nu_{T,k-1} \mathbb{G}_{k-1}^H, \mathbb{D}(\mathbf{v}^h)) \right] + \theta_3 \Delta t_k (\mathbf{f}_{k-1}, \mathbf{v}^h) + \theta_4 \Delta t_k (\mathbf{f}_k, \mathbf{v}^h), \quad \forall \mathbf{v}^h \in V^h, \\
0 & = (q^h, \nabla \cdot \mathbf{u}_k^h), \quad \forall q^h \in Q^h, \\
0 & = (\mathbb{G}_k^H - \mathbb{D}(\mathbf{u}_k^h), \mathbb{L}^H), \quad \forall \mathbb{L}^H \in L^H,
\end{aligned} \tag{3}$$

with $\Delta t_k = t_k - t_{k-1}$. We will use in our studies the Crank–Nicolson scheme, $\theta_1 = \theta_2 = \theta_3 = \theta_4 = 0.5$, since this scheme has been proven to be a good compromise between accuracy and efficiency [16, 24].

For the main features of an efficient implementation of the fully implicit approach we refer to [18].

3 The Projection–Based Finite Element Variational Multiscale Method With an Adaptively Chosen Large Scale Space

The projection–based FEVMS method requires the choice of the tensor–valued large scale space L^H in order to define the projection. In [18] it has been shown that an efficient implementation of the one–level method requires this space to consist of discontinuous functions. This is also understandable from the fact that the resolved small scales are the projection of an already discontinuous function, namely the deformation tensor of the finite element velocity. In [18, 25, 20, 21] numerical studies were performed for $L^H = P_0$ and $L^H = P_1^{\text{disc}}$. In the adaptive FEVMS method, L^H is allowed to possess different polynomial degrees on different mesh cells. The more turbulence a region presents, the stronger the influence of the turbulence model will be and the local polynomial degree for L^H increases as the amount of turbulence decreases. In regions with strong turbulence, e.g. along the boundary of the domain, a turbulence model is necessary, often in contrast to the interior of the domain. The amount of turbulence and in consequence the local polynomial degree of L^H will be controlled a posteriorily by the local L^2 –norm of the resolved small scales $\mathbb{G}^H - \mathbb{D}(\mathbf{u}^h)$.

In order to obtain information about the amount of turbulence, the size of the resolved small scales

$$\eta_K = \frac{\|\mathbb{G}^H - \mathbb{D}(\mathbf{u}^h)\|_{L^2(K)}}{\|1\|_{L^2(K)}} = \frac{\|\mathbb{G}^H - \mathbb{D}(\mathbf{u}^h)\|_{L^2(K)}}{|K|^{1/2}}, \quad K \in \mathcal{T}^h, \tag{4}$$

where K is a mesh cell of the triangulation \mathcal{T}^h , is compared to a mean resolved small scale size. The size of the resolved small scales does not depend on the size of the mesh cells and with definition (4) the size of the mesh cells scales out. In the cells where the size of the resolved small scales η_K is (very) large compared with the mean resolved small scale size, high turbulence occurs, whereas in cells where η_K is smaller than the mean, i.e. there is little variance in the size of the resolved small scales, the amount of turbulence is low. In the numerical studies presented in Section 4, three possible definitions of means will be studied:

$$\bar{\eta} := \frac{1}{\text{no. of cells}} \sum_{K \in \mathcal{T}^h} \eta_K, \quad \text{the mean over all mesh cells, (mean),} \quad (5)$$

$$\bar{\eta}^t := \frac{1}{\text{no. of time steps}} \sum_{\text{time steps}} \bar{\eta}, \quad \text{time average, (mean_time),} \quad (6)$$

$$\bar{\eta}^{t/2} := \frac{\bar{\eta} + \bar{\eta}^t}{2}, \quad \text{(mean_mean).} \quad (7)$$

Of course, considering time averages makes sense only if main features of the flow, like the inflow velocity, do not change much during the simulation. Another possibility for defining a time average would be the consideration of a prescribed number of last time steps instead of all time steps.

Four different types of turbulence regions will be considered. For very large η_K , $K \in \mathcal{T}^h$, the eddy viscosity model should be applied locally to all resolved scales. This corresponds to choosing $L^H(K)$ to be the space consisting only of the zero tensor, denoted by $P_{00}(K)$. Otherwise, $L^H(K)$ can be chosen to be $P_0(K)$, $P_1^{\text{disc}}(K)$, or $P_2^{\text{disc}}(K)$, corresponding to large, small and respectively very small η_K . The choice $P_2^{\text{disc}}(K)$ corresponds (almost) to switching off the turbulence model. There are very few scales left in $\mathbb{G}^H - \mathbb{D}(\mathbf{u}^h)$ in this case. Since we think that the possibility of switching off the turbulence model should be available in the method, we set $\nu_T = 0$ in the case of very small η_K . In more detail, regarding the definition of the four turbulence regions, consider $C_1 \leq C_2 \leq C_3$, all non-negative, and denote by η the ratio between η_K and one of the means above, then $L^H(K)$ will be chosen as follows:

1. for cells K with $\eta \leq C_1$: $L^H(K) = P_2^{\text{disc}}(K)$, $\nu_T(K) = 0$,
2. for cells K with $C_1 < \eta \leq C_2$: $L^H(K) = P_1^{\text{disc}}(K)$,
3. for cells K with $C_2 < \eta \leq C_3$: $L^H(K) = P_0(K)$,
4. for cells K with $C_3 < \eta$: $L^H(K) = P_{00}(K)$.

In the numerical simulations, together with the three different means, different values for C_1 , C_2 , C_3 will be studied.

Another parameter in the adaptive method is the number of time steps n_{update} after which the space L^H will be updated. This can be done after each time step but also after a prescribed number of time steps only.

4 Numerical Studies

We will consider two examples in the numerical studies, a strongly underresolved turbulent channel flow and a turbulent flow around a cylinder. The Q_2/P_1^{disc} pair of finite element spaces was used for velocity and pressure in all simulations presented below. This pair of finite elements is among the best performing ones for incompressible flow simulations [9, 14, 16]. All simulations were performed with the code MooNMD [23].

4.1 The turbulent channel flow at $Re_\tau = 180$

Turbulent channel flows are standard benchmark problems for turbulent flow simulations. These flows are statistically steady-state. The turbulent channel flow at $Re_\tau = 180$ was defined in [28] where also reference values for time and space averaged flow quantities are given. The setup of this problem for the projection-based FEVMS method is presented in detail in [25].

The numerical studies at the turbulent channel flow should be considered as a proof of concept. Firstly, it will be demonstrated that (4) gives appropriate information for the appearance of turbulence such that $L^H(K)$ is chosen in a way which can be expected. Secondly, the different possibilities (5) – (7) for defining a mean value of η_K will be studied, several choices of the parameters C_1, C_2, C_3 and the effect of the frequency of updating the space L^H , n_{update} , on the results of the adaptive method will be investigated. Comparisons with simulations with uniform spaces L^H will be presented as well.

The flow is given in $\Omega = (-2\pi, 2\pi) \times (0, 2) \times (-2\pi/3, 2\pi/3)$ with periodic boundary conditions in streamwise and spanwise direction. At the walls $y = 0$ and $y = 2$, no-slip boundary conditions are described. We will consider this flow on a very coarse grid. This corresponds to a typical situation in applications where the grid size is often coarser by magnitudes than the size of the smallest scales. The grid consists of $8 \times 16 \times 8 = 1024$ mesh cells, which results in 25 344 velocity degrees of freedom and in 4096 pressure degrees of freedom. It is uniform in streamwise and spanwise direction but anisotropic in wall normal direction where the grid points are distributed accordingly to

$$y_i = 1 - \cos\left(\frac{i\pi}{N_y}\right), \quad i = 0, \dots, 16.$$

As eddy viscosity model, we used the van Driest damping of the Smagorinsky model [32, 2]

$$\nu_T = 0.01(2h_{K,\min})^2 \|\mathbb{D}(\mathbf{u}^h)\|_F \begin{cases} \left(1 - \exp\left(\frac{-y^+}{A}\right)\right)^2, & y^+ < 5, \\ 1 & \text{else,} \end{cases} \quad (8)$$

with $h_{K,\min}$ being the shortest edge of a mesh cell K , $\|\cdot\|_F$ being the Frobenius norm, $A = 26$ and $y^+ = Re_\tau y = 180y$ being the distance from the wall measured in wall units (or viscous lengths). All simulations started with a fully developed flow field. Initially, $L^H(K) = P_0(K)$ was chosen for all mesh cells. We allowed the simulations 10 seconds to

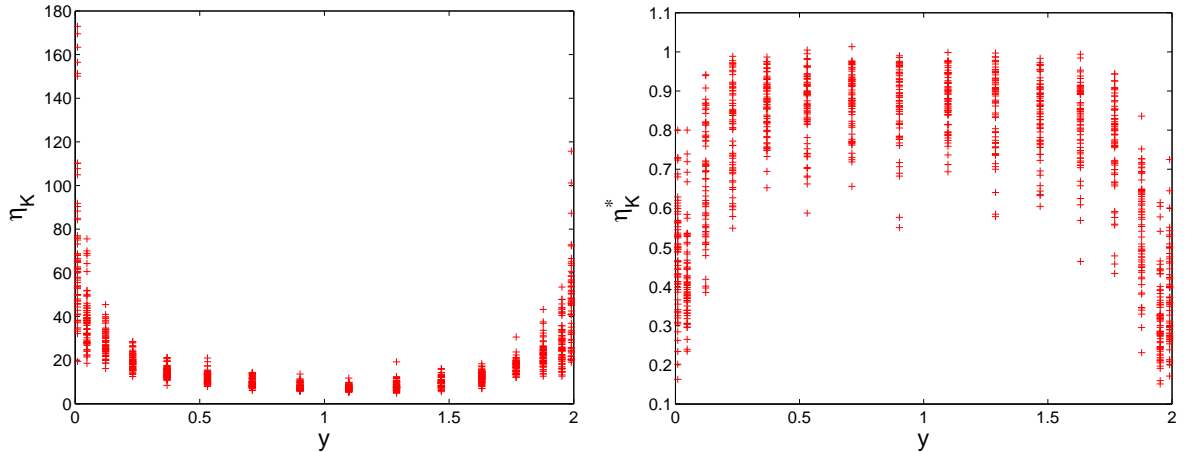


Figure 1: Turbulent channel flow. Size of η_K computed with (4) (left) and size of (9) (right) in a simulation with $L^H = P_0$. The y -coordinate is the x -coordinate of the barycenter of the mesh cells.

develop with the parameters (8) and the adaptive strategy for choosing L^H . The time-averages presented below were computed in another 30 seconds. The Crank–Nicolson scheme was applied with the equidistant time step $\Delta t = 0.004$. This is smaller than the Kolmogorov time scale and it fits into the range of the time step proposed in [4]. Below, comparisons of the mean velocity profile U_{mean}^h and the rms turbulence intensity $u_{\text{rms}}^{h,*}$ with the data from [28] are given. The computed mean values are the average of the mean values of the lower and upper half of the channel. For details of the computations of these quantities, we refer to [25].

Besides the $L^2(K)$ -norm of the resolved small scales (4), one could think that also the ratio of this norm to the $L^2(K)$ -norm of all resolved scales

$$\eta_K^* = \frac{\|\mathbb{G}^H - \mathbb{D}(\mathbf{u}^h)\|_{L^2(K)}}{\|\mathbb{D}(\mathbf{u}^h)\|_{L^2(K)}}, \quad K \in \mathcal{T}^h, \quad (9)$$

might be an appropriate measure for the intensity of the local turbulence. In turbulent channel flows, a strong turbulence can be expected at the walls. Fig. 1 shows typical snapshots of spatial distributions with respect to the wall normal direction of (4) and (9). Each column in the pictures shows the values of all mesh cells with the respective y -coordinate of the barycenter. The values of η_K at the walls, which are located at $y = 0$ and $y = 2$, are very large compared with the values in the center of the channel. In contrast, the values of η_K^* are rather equidistributed in the channel. Thus, it is possible to derive from (4) the correct information about the size of the local turbulence but not from (9). We performed numerous simulations with different parameters in the adaptive method for choosing L^H . For shortness of presentation, only representative results are given below. Results obtained with the definitions (5) – (7) of the mean values, for a fixed set of parameters C_1, C_2, C_3 and a fixed number of time steps $n_{\text{update}} = 10$ to update L^H , are presented

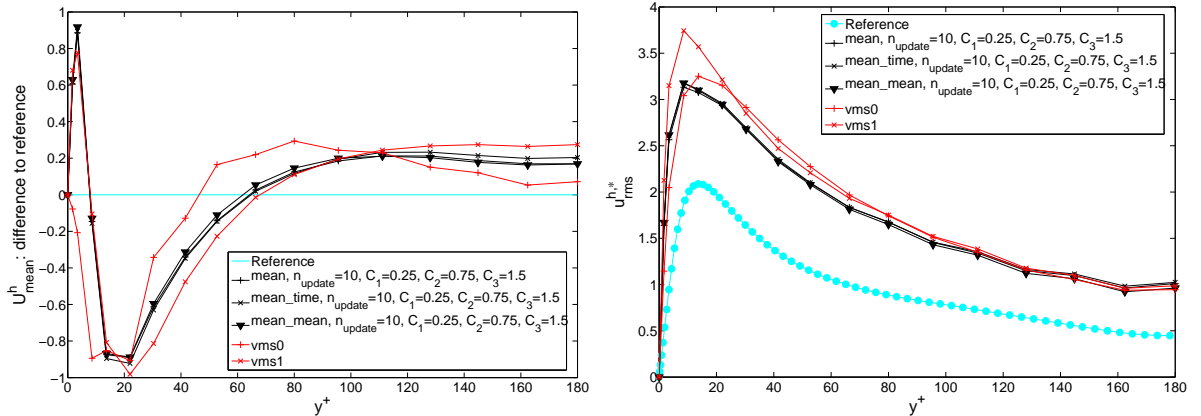


Figure 2: Turbulent channel flow. Difference to the mean velocity and the rms intensities for using different methods for computing mean values in the adaptive method for choosing L^H .

in Fig. 2. In addition, results obtained with the fixed a priori choices $L^H = P_0$ (vms0) and $L^H = P_1^{\text{disc}}$ (vms1) are shown. It can be observed that there are only very slight differences in the curves with the different mean values. The rms turbulence intensity is overpredicted in all simulations. The overprediction of second order statistics is typically observed in turbulent channel flow simulations with low order discretizations like finite elements or finite volumes on coarse grids [8, 7, 25, 20].

The choice of the parameters C_1 and C_2 has a much stronger effect on the results than the choice of the mean value, see Fig. 3. Generally, the adaptive method works the following way: the larger the values C_1, C_2, C_3 , the larger the space L^H becomes and the less eddy viscosity is introduced into the simulations. The results presented in Fig. 3 show that in this example the values $C_1 \in \{0.2, 0.3\}$ and $C_2 \in \{0.5, 0.75\}$ lead to the best results. The value of C_3 has comparatively little influence. For $C_3 \geq 2$, the curves are almost identical if all other parameters in the simulations were chosen to be the same.

Figure 4 presents results with different numbers of time steps between the updates of L^H . With respect to this parameter, there are only slight differences in the curves. This parameter plays for simulations of the statistically steady-state turbulent channel flows obviously a minor role.

Appropriate choices of the parameters in the adaptive method lead with respect to the mean velocity profile to somewhat more accurate results than both fixed choices of the large scale space. All results with the adaptive method are more accurate than the results with $L^H = P_1^{\text{disc}}$ with respect to $u_{\text{rms}}^{h,*}$.

Finally, we like to illustrate the form of the large scale space L^H obtained with the adaptive method. Fig. 5 shows adaptively chosen spaces for two sets of parameters C_1, C_2, C_3 . One can observe that at the walls locally small spaces for $L^H(K)$ were chosen whereas the eddy viscosity model was switched off in the center of the channel.

Fig. 6 illustrates the development of the size (number of degrees of freedom) of the space L^H for different parameters C_1, C_2, C_3 and n_{update} .

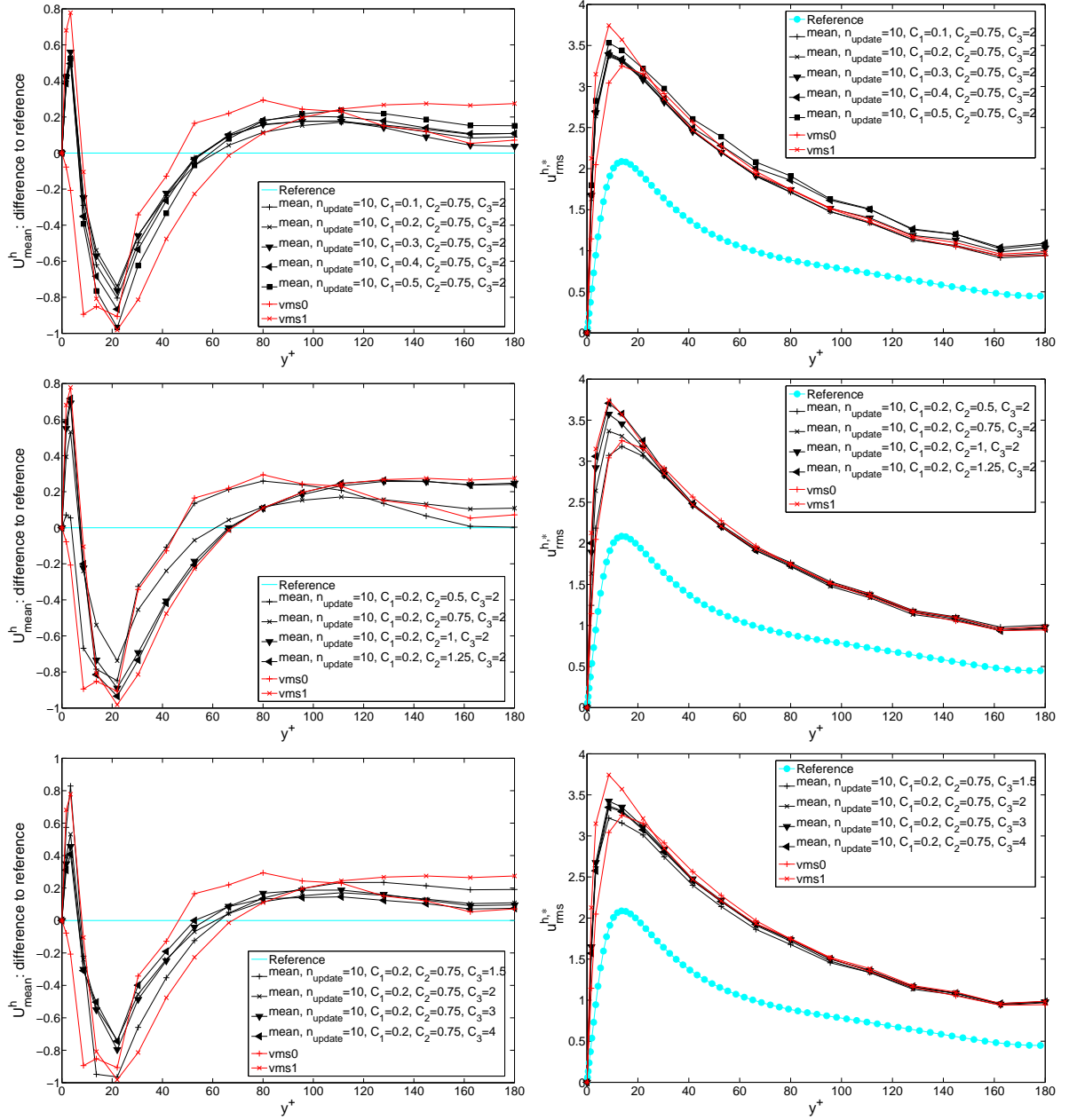


Figure 3: Turbulent channel flow. Difference to the mean velocity and the rms intensities for using different sets of constants in the adaptive method for choosing L^H .

4.2 Turbulent flow around a cylinder with square cross section at $Re = 22000$

This example was defined in [29]. The flow domain and the initial grid (level 0) consisting of hexahedra are presented in Fig. 7. We performed the simulations on level 2, resulting in 522 720 velocity degrees of freedom and 81 920 pressure degrees of freedom. The inflow

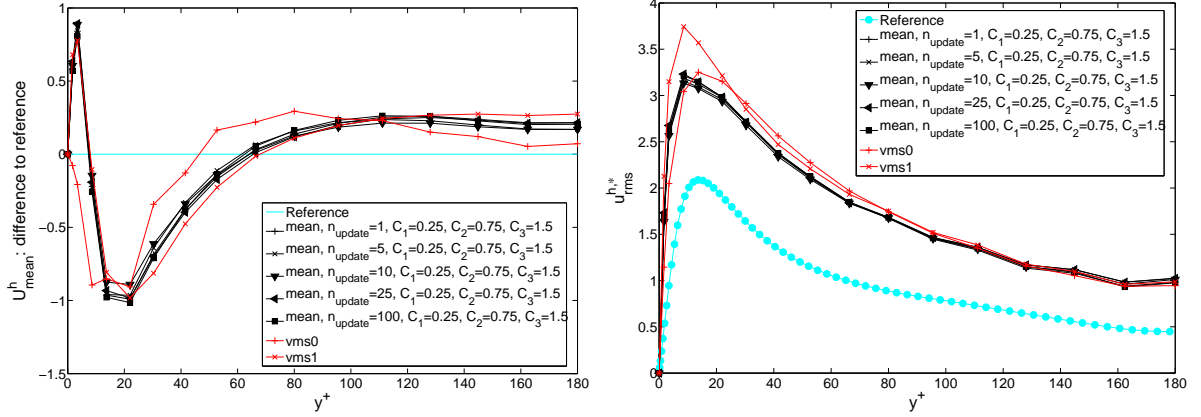


Figure 4: Turbulent channel flow. Difference to the mean velocity and the rms intensities for using different numbers of time steps n_{update} for updating L^H .

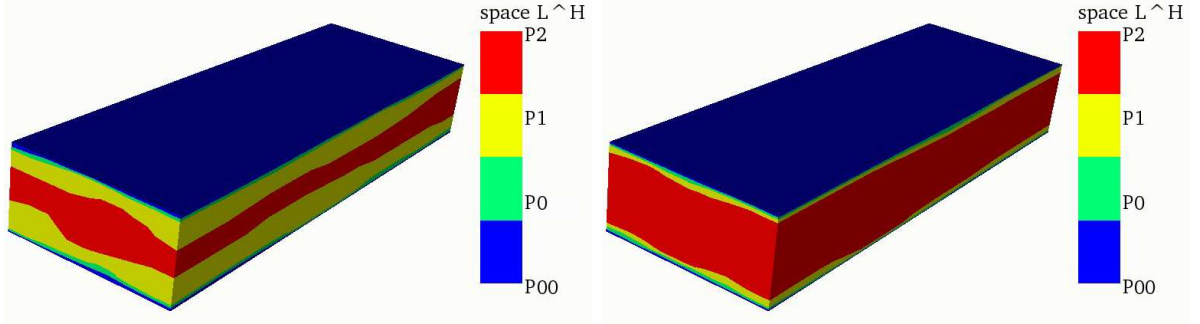


Figure 5: Turbulent channel flow. Snapshots of L^H ; left: $C_1 = 0.25, C_2 = 0.75, C_3 = 1.5$; right: $C_1 = 0.5, C_2 = 1, C_3 = 2$.

is prescribed by

$$\mathbf{u}(t, 0, y, z) = (1 + 0.04 \text{ rand}, 0, 0)^T,$$

where rand is a random number in $[-0.5, 0.5]$. The noise in the inflow serves to stimulate the turbulence. No-slip boundary conditions were prescribed at the column. Outflow boundary conditions were set at $x = 2.5$. On all other boundaries, free slip conditions were used. The Reynolds number of the flow, based on the mean inflow $U_\infty = 1 \text{ m/s}$, the length of the cylinder $D = 0.1 \text{ m}$ and the viscosity $\nu = 1/220\,000$ is $Re = 22\,000$. There are no external forces acting on the flow.

The Crank-Nicolson scheme was applied with equidistant time steps of length $\Delta t = 0.005$. Again, the Smagorinsky model

$$\nu_T = 0.01(2h_{K,\min})^2 \|\mathbb{D}(\mathbf{u}^h)\|_F$$

was used as eddy viscosity model.

This example describes a statistically periodic flow. Functionals of interest of the flow are the drag and the lift coefficient at the cylinder and the Strouhal number. The coefficients

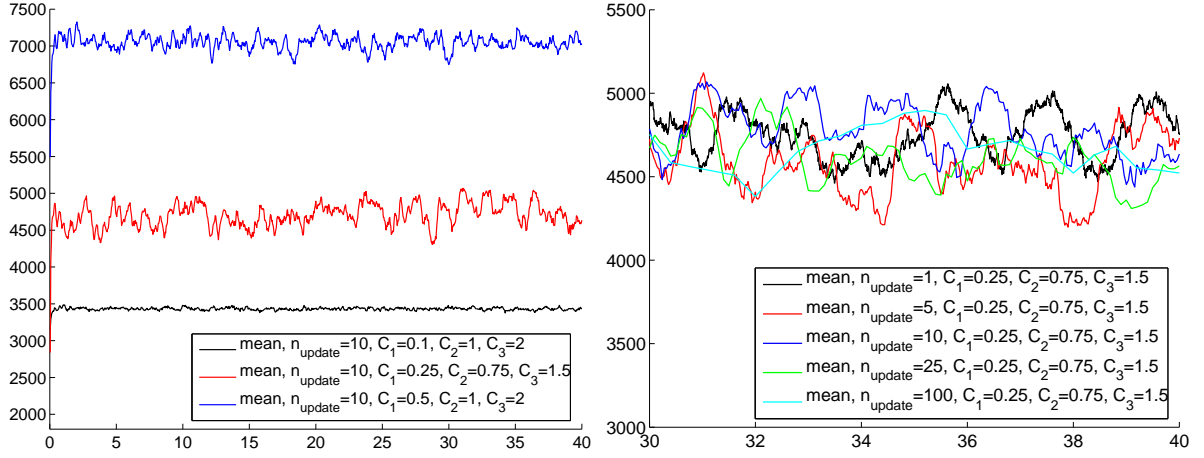


Figure 6: Turbulent channel flow. Development of the size of L^H (number of degrees of freedom); left: different sets of constants in the adaptive method for L^H ; right: different number of time steps between updates of L^H .

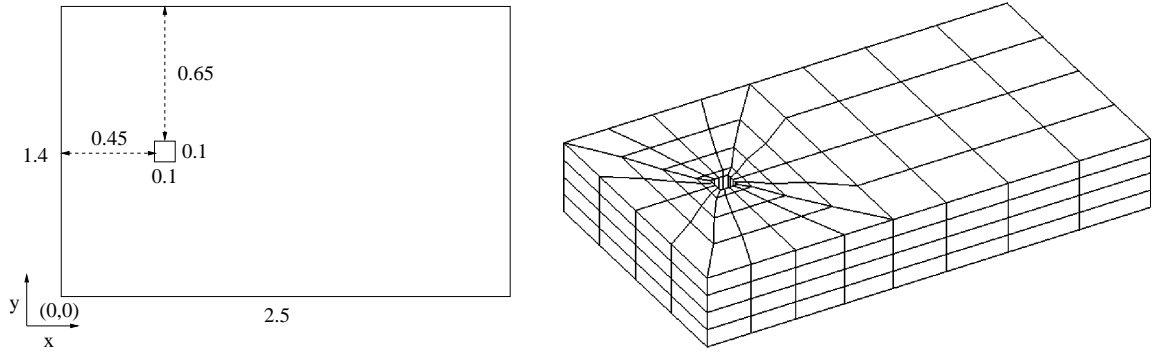


Figure 7: Turbulent flow around a cylinder with square cross section. left: the cross section of the domain (all length in m), the height of the channel is $H = 0.4 m$; right: initial grid.

can be computed as volume integrals, e.g., see [15],

$$c_d(t) = -\frac{2}{\rho DHU_\infty^2} \left[(\mathbf{u}_t, \mathbf{v}_d) + (\nu \nabla \mathbf{u}, \nabla \mathbf{v}_d) + b(\mathbf{u}, \mathbf{u}, \mathbf{v}_d) - (p, \nabla \cdot \mathbf{v}_d) \right]$$

for any function $\mathbf{v}_d \in (H^1(\Omega))^3$ with $(\mathbf{v}_d)|_S = (1, 0, 0)^T$, \mathbf{v}_d vanishes on all other boundaries and S is the boundary of the cylinder. The density of the fluid is in this example $\rho = 1 \text{ kg/m}^3$. Similarly, it holds

$$c_l(t) = -\frac{2}{\rho DHU_\infty^2} \left[(\mathbf{u}_t, \mathbf{v}_l) + (\nu \nabla \mathbf{u}, \nabla \mathbf{v}_l) + b(\mathbf{u}, \mathbf{u}, \mathbf{v}_l) - (p, \nabla \cdot \mathbf{v}_l) \right]$$

for any function $\mathbf{v}_l \in (H^1(\Omega))^3$ with $(\mathbf{v}_l)|_S = (0, 1, 0)^T$ and \mathbf{v}_l vanishes on all other boundaries. The actual choice of \mathbf{v}_d and \mathbf{v}_l in our computations is the same as in [22]. The

Strouhal number is defined by $St = DU_\infty/T$, where T is a characteristic time scale (the average length of a period in this example). Below, time-averaged drag and lift coefficients, \bar{c}_d and \bar{c}_l , root mean squared (rms) values for c_d , c_l which are defined by

$$c_{d,\text{rms}} = \left(\sum_i (c_d(t_i) - \bar{c}_d)^2 \right)^{1/2}, \quad c_{l,\text{rms}} = \left(\sum_i (c_l(t_i) - \bar{c}_l)^2 \right)^{1/2},$$

where the summation covers all discrete times in the time interval for which \bar{c}_d, \bar{c}_l are computed, and the Strouhal number are presented.

All computations started with a fully developed flow field. After allowing the flows 20 seconds for developing with respect to the used method, the time averages were computed using the data of the following 25 full periods. The begin of a period is defined by c_l changing from negative to positive values.

Table 1: Turbulent flow around a cylinder, time-averaged functionals of interest and corresponding rms values.

C_1	C_2	C_3	mean	\bar{c}_l	$c_{l,\text{rms}}$	\bar{c}_d	$c_{d,\text{rms}}$	St
VMS with $L^H = P_0$				0.004	1.190	2.590	0.1734	0.1434
VMS with $L^H = P_1^{\text{disc}}$				blow up of the solver				
0.1	0.50	3	$\bar{\eta}$	0.018	1.280	2.593	0.1274	0.1395
0.1	1.00	3	$\bar{\eta}$	-0.015	1.427	2.649	0.1216	0.1432
0.2	1.00	3	$\bar{\eta}$	0.023	1.289	2.566	0.1512	0.1386
0.2	1.00	3	$\bar{\eta}^{t/2}$	-0.028	1.310	2.593	0.1233	0.1404
0.3	0.75	2	$\bar{\eta}$	-0.024	1.386	2.612	0.1145	0.1443
0.3	1.00	2	$\bar{\eta}$	0.029	1.205	2.536	0.1756	0.1387
0.3	1.25	2	$\bar{\eta}$	-0.029	1.381	2.612	0.1439	0.1455
0.3	1.00	3	$\bar{\eta}$	-0.029	1.362	2.614	0.1202	0.1394
0.5	1.00	2	$\bar{\eta}$	0.007	1.395	2.596	0.1665	0.1447
0.5	1.25	2	$\bar{\eta}$	-0.028	1.435	2.589	0.1706	0.1444
experiments					0.7–1.4	1.9–2.1	0.1–0.2	0.1320

Results of our simulations are presented in Table 1. All simulations with the adaptive VMS method were performed with $n_{\text{update}} = 10$. The simulations with $L^H = P_1^{\text{disc}}$ for all times blew up in finite time, i.e. our solver diverged. We tried to stabilize the solver in several ways, however without success. We think that the reason for the blow-up is that the VMS with P_1^{disc} does not introduce sufficient viscosity into the model. Experimental values, from [29], are given as comparison with the values obtained with the numerical simulations. One can observe that \bar{c}_l is close to zero for all simulations, $c_{l,\text{rms}}$ is within the experimental range for most of the simulations and $c_{d,\text{rms}}$ for all simulations. The overprediction of \bar{c}_d was observed already for many codes used in the comparative study from [29]. The quantity easiest to compare with is the Strouhal number. Table 1 shows

that the VMS method with adaptive large scale space gives better results than VMS with $L^H = P_0$ for appropriate chosen parameters: $C_1 \in \{0.2, 0.3\}$, $C_2 = 1$. Again, the choice of C_3 is of minor importance. Thus, the range of appropriate parameters is similar to the one in the turbulent channel flow problem. An exemplary comparison shows that the use of different mean values leads to notable differences in the results.

A typical snapshot of the distribution of the resolved small scales and the corresponding space L^H is presented in Fig. 8. Also for the turbulent flow around a cylinder, the large scale space is chosen in such a way that the eddy viscosity model becomes effective only where turbulence occurs: at the cylinder and downstream the cylinder.

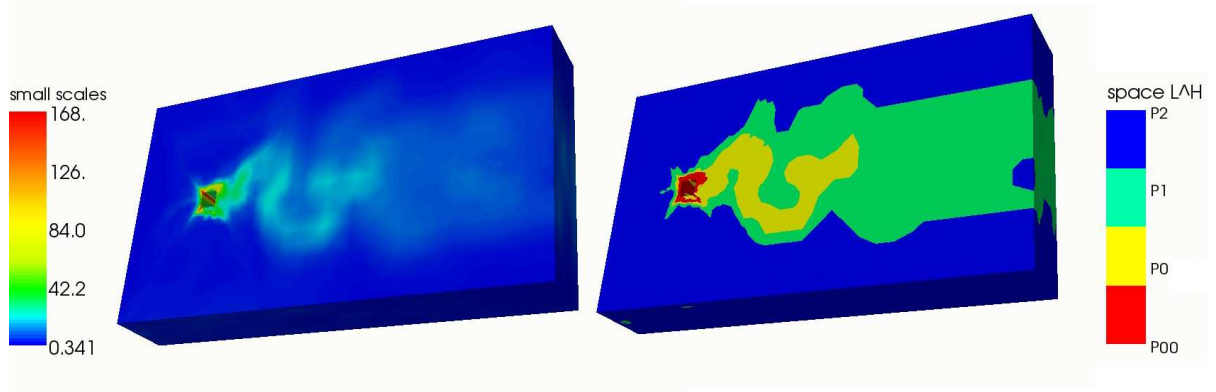


Figure 8: Turbulent flow around a cylinder, snapshot of η_K and L^H , $C_1 = 0.3$, $C_2 = 1$, $C_3 = 3$.

5 Summary

The paper presented a three-level finite element variational multiscale method for turbulent flow simulations with an adaptive choice of the large scale space. The adaption is based on the size of the computed resolved small scales. Simulations were performed for a turbulent channel flow and a turbulent flow around a cylinder.

It was demonstrated that the method chooses the large scale space in an appropriate way, i.e. the effect of the turbulence model is controlled by the size of the local turbulence intensity. Compared with choosing the same large scale space in all mesh cells and for all times, it was shown that appropriate choices of parameters in the adaptive method lead to improvements of the results.

The presented numerical studies give first guidelines on the importance of the parameters and their appropriate choice. Further studies, also at different flows, have to refine these guidelines.

Acknowledgment. The research of A. Kindl was supported by the Deutsche Forschungsgemeinschaft (DFG) by grant No. Jo 329/7-2.

References

- [1] L. BERSELLI, C. GRISANTI, AND V. JOHN, *Analysis of commutation errors for functions with low regularity*, J. Comp. Appl. Math., 206 (2007), pp. 1027 – 1045.
- [2] L. BERSELLI, T. ILIESCU, AND W. LAYTON, *Mathematics of Large Eddy Simulation of Turbulent Flows*, Springer Verlag, 2006.
- [3] L. BERSELLI AND V. JOHN, *Asymptotic behavior of commutation errors and the divergence of the reynolds stress tensor near the wall in the turbulent channel flow*, Math. Meth. Appl. Sci., 29 (2006), pp. 1709 – 1719.
- [4] H. CHOI AND P. MOIN, *Effects of the computational time step on numerical solutions of turbulent flow*, J. Comp. Phys., 113 (1994), pp. 1 – 4.
- [5] A. DUNCA, V. JOHN, AND W. LAYTON, *The commutation error of the space averaged Navier-Stokes equations on a bounded domain*, in Contributions to Current Challenges in Mathematical Fluid Mechanics, J. H. G.P. Galdi and R. Rannacher, eds., Birkhäuser, 2004, pp. 53 – 78.
- [6] M. GERMANO, U. PIOMELLI, P. MOIN, AND W. CABOT, *A dynamic subgrid-scale eddy viscosity model*, Phys. Fluids A, 3 (1991), pp. 1760 – 1765.
- [7] V. GRAVEMEIER, *A consistent dynamic localization model for large eddy simulation of turbulent flows based on a variational formulation*, J. Comp. Phys., 218 (2006), pp. 677 – 701.
- [8] ———, *Scale-separating operators for variational multiscale large eddy simulation of turbulent flows*, J. Comp. Phys., 212 (2006), pp. 400 – 435.
- [9] P. GRESHO AND R. SANI, *Incompressible Flow and the Finite Element Method*, Wiley, Chichester, 2000.
- [10] J.-L. GUERMOND, *Stabilization of Galerkin approximations of transport equations by subgrid modeling*, M2AN, 33 (1999), pp. 1293 – 1316.
- [11] T. HUGHES, *Multiscale phenomena: Green's functions, the Dirichlet-to-Neumann formulation, subgrid-scale models, bubbles and the origin of stabilized methods*, Comp. Meth. Appl. Mech. Engrg., 127 (1995), pp. 387 – 401.
- [12] T. HUGHES, L. MAZZEI, AND K. JANSEN, *Large eddy simulation and the variational multiscale method*, Comput. Visual. Sci., 3 (2000), pp. 47 – 59.
- [13] T. HUGHES, G. SCOVAZZI, AND L. FRANCA, *Multiscale and stabilized methods*, in Encyclopedia of Computational Mechanics, E. Stein, R. de Borst, and T. Hughes, eds., John Wiley & Sons, 2004.

- [14] V. JOHN, *Higher order finite element methods and multigrid solvers in a benchmark problem for the 3D Navier-Stokes equations*, Int. J. Num. Meth. Fluids, 40 (2002), pp. 775 – 798.
- [15] ———, *Large Eddy Simulation of Turbulent Incompressible Flows. Analytical and Numerical Results for a Class of LES Models*, vol. 34 of Lecture Notes in Computational Science and Engineering, Springer-Verlag Berlin, Heidelberg, New York, 2004.
- [16] ———, *Reference values for drag and lift of a two-dimensional time dependent flow around a cylinder*, Int. J. Numer. Meth. Fluids, 44 (2004), pp. 777 – 788.
- [17] ———, *On large eddy simulation and variational multiscale methods in the numerical simulation of turbulent incompressible flows*, Appl. of Math., 51 (2006), pp. 321 – 353.
- [18] V. JOHN AND S. KAYA, *A finite element variational multiscale method for the Navier-Stokes equations*, SIAM J. Sci. Comp., 26 (2005), pp. 1485 – 1503.
- [19] V. JOHN, S. KAYA, AND W. LAYTON, *A two-level variational multiscale method for convection-dominated convection-diffusion equations*, Comp. Meth. Appl. Math. Engrg., 195 (2006), pp. 4594 – 4603.
- [20] V. JOHN AND A. KINDL, *Variants of projection-based finite element variational multiscale methods for the simulation of turbulent flows*, Int. J. Numer. Meth. Fluids, 56 (2008), pp. 1321 – 1328.
- [21] ———, *Numerical studies of finite element variational methods for turbulent flow simulations*, Comput. Methods Appl. Mech. Engrg., (2009). in press.
- [22] V. JOHN AND G. MATTHIES, *Higher order finite element discretizations in a benchmark problem for incompressible flows*, Int. J. Num. Meth. Fluids, 37 (2001), pp. 885 – 903.
- [23] ———, *MooNMD - a program package based on mapped finite element methods*, Comput. Visual. Sci., 6 (2004), pp. 163 – 170.
- [24] V. JOHN, G. MATTHIES, AND J. RANG, *A comparison of time-discretization/linearization approaches for the time-dependent incompressible Navier-Stokes equations*, Comput. Methods Appl. Mech. Engrg., 195 (2006), pp. 5995 – 6010.
- [25] V. JOHN AND M. ROLAND, *Simulations of the turbulent channel flow at $Re_\tau = 180$ with projection-based finite element variational multiscale methods*, Int. J. Numer. Meth. Fluids, 55 (2007), pp. 407 – 429.
- [26] D. LILLY, *A proposed modification of the Germano subgrid-scale closure method*, Phys. Fluids A, 4 (1992), pp. 633 – 635.

- [27] B. MOHAMMADI AND O. PIRONNEAU, *Analysis of the K-Epsilon Turbulence Model*, John Wiley & Sons, 1994.
- [28] D. MOSER, J. KIM, AND N. MANSOUR, *Direct numerical simulation of turbulent channel flow up to $Re_\tau = 590$* , *Phys. Fluids*, 11 (1999), pp. 943 – 945.
- [29] W. RODI, J. FERZIGER, M. BREUER, AND M. POURQUIÉ, *Status of large eddy simulation: Results of a workshop*, *Journal of Fluids Engineering*, 119 (1997), pp. 248 – 262.
- [30] P. SAGAUT, *Large Eddy Simulation for Incompressible Flows*, Springer-Verlag, Berlin, Heidelberg New York, 3rd ed., 2006.
- [31] J. SMAGORINSKY, *General circulation experiments with the primitive equations*, *Mon. Weather Review*, 91 (1963), pp. 99 – 164.
- [32] E. VAN DRIEST, *On turbulent flow near a wall*, *J. Aerospace Sci.*, 23 (1956), pp. 1007 – 1011.